



W. W. Hansen Experimental Physics Laboratory

STANFORD UNIVERSITY  
STANFORD, CALIFORNIA 94305 - 4085


Gravity Probe B Relativity Mission

## SCIENCE DOCUMENT FOR

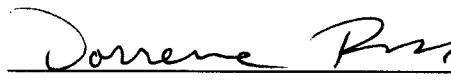
### Test of Telescope #3


GP-B S0300    Rev B

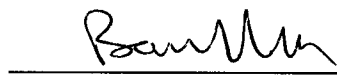
April 22, 2002

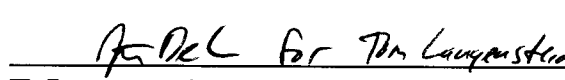
  
Prepared by: Suwen Wang  
Test Engineer  
Date 4/25/02

  
Approved by: M. Keiser  
Chief Scientist  
Date 4/25/02

  
Approved by: D. Ross  
Quality Assurance  
Date 4/25/02

  
Approved by: R. Whelan  
Systems Engineering  
Date 4/25/02

  
Approved by: B. Muhlfelder  
Hardware Manager  
Date 4/25/02

  
T. Langenstein  
Date 4/25/02

ITAR Assessment Performed

ITAR Control Required

\_\_\_\_ YES

☒ NO

**GP-B Science Document 0300**

## Table of Contents

Revision Sheet.....	i
List of Tables .....	ii
List of Figures .....	iii
Introduction.....	1
Integration.....	1
Room Temperature Test.....	1
Low Temperature Test.....	2
Telescope Field of View.....	3
Telescope Saturation Range.....	3
Telescope Perpendicularity of Readout Axes.....	4
Telescope Linearity.....	4
Telescope Strehl Ratio.....	4
Telescope Scale Factor.....	5
Telescope Optical Transmission.....	5
Telescope Orientation of Reticle Reflecting Surface.....	6
Misalignment of Optical Center from Center of Aperture Stop.....	6
Telescope Readout Noise Performance and Related Telescope Data.....	7
Discrepancies Observed.....	7
Summary.....	9
Appendix A. Telescope Detector Assignment and Scan Coordinate Cross Reference....	10

## REVISION SHEET

1. Rev.- 15 June1998
2. Rev. A 12 February 1999 Add figures
- 3.Rev. B 22 April 2002 Up date of “Telescope Perpendicularity of Readout Axes” results.  
Reference page 4

List of Tables

Table 1 Peak Intensity Distribution of All Detectors .....8

Table 1A Cross Reference .....10

## List of Figures

Figure 1A Tel#3 Room temperature Test,2/20/98.....	12
Figure 2A Tel#3 Room temperature Test,2/24/98.....	13
Figure 3 Tel#3 Focal Test,RT, 3/3//98.....	14
Figure 4B Telescope#3 Field of View Scan, Room Temperature.....	15
Figure 5A Telescope#3 Saturation Range, Room Temperature.....	16
Figure 6A Tel#3 Wide Field Scan, 4K, 3/12/98.....	17
Figure 7A Tel#3 Narrow Field Scan, 4K, 3/25/98.....	18
Figure 8 Tel#3 Focal Test, 4K, 3/27/98.....	19
Figure 9B Tel#3 Field Scan, 4K.....	20
Figure 10B Telescope#3 Saturation Range test 4K.....	21
Figure 11B Telescope Scale Factor Test,4K scan_y10_04/11/98.igr.....	22
Figure 12A Telescope #3 Test Artificial Star#2 Intensity Measurement 4/30/98.....	23
Figure 13 Telescope #3 Readout Noise Measurement Tel#3_RNM_analysis.igr, 4/08/98.....	24
Figure 14 Low Light Intensity Test.....	25

## Test of Telescope #3

### Introduction

This report is a summary of tests performed on Telescope #3 with artificial star #2. It will nominally follow the order the tests were performed. In the low temperature test section, those tests which directly provides results to meet the T003 or SIA specs will have titles highlighted in bold face and specs in italics.

### Integration

The integration of Telescope #3 into Telescope Probe #2 started on Feb. 3, 1998.

The DPA cables were found to be not compatible with the telescope test probe. Two of the ribbon cables were bent 180 degrees with Allen key and fingers to accommodate the mismatch.

The first integration was complete on Feb. 7, 1998.

Two broken wires were found on the feedthrough for the channel B reflected channels on Feb. 9 and the feed through replaced with a spare.

Two shorts were found on the feedthrough for the channel A transmitted channels on Feb. 10 and the feed through replaced with another spare.

The integration process was completed with no further problems on Feb. 11, 1998.

### Room Temperature Test

The telescope readout electronics was delivered on Feb. 20, 1998.

Due to the leakage of the photo diodes at room temperature, 20.0 mA of driving current is used for the laser diode of the star light source during the entire test process except for a few special occasions. This driving current ensures that the room temperature leakage current is about the same as the signal level and no ramping saturation is observed.

For a cross reference of the detector assignment and scan coordinates, see appendix A.

A raster scan was performed with a range of 260 x 260 arc secs in grid sizes of 5.2 x 5.2 arc secs. A typical scan results is shown in fig. 1a. and 1b. The notation convention is such that the legend to the right is for the graph to the right and the legend on the upper line correspond to graphs on the upper side. For a complete collection of all the results in the scan, see GP-B, P0225 attachment. Two undesirable features are observed in the result observed here. First, a sloped top is observed in fig. 1b. This sloped top is observed in all the Y axis detectors. Second, the maximum photo current is different for different detectors. Both of these issues will be addressed later.

A second set of raster scans was performed with a range of 10 x 10 arc secs in grid sizes of 0.2 arc secs centered nominally on the optical axis. Typical results are shown in fig. 2a and fig. 2b with complete set attached to P0227. These results show no unwanted behavior other than the maximum intensity difference mentioned earlier.

A focal scan is performed by adjusting the position of the fiber end of the artificial star along the optical axis to make the outgoing beam deviate from a collimated beam. This adjusted amount is converted to the focal point position of the telescope with respect to the roof edge. Fig. 3 shows the result of a focal scan. This graph shows the maximum of the signal slope as a function of the focal point position. The zero focal position also corresponds to the star beam being well collimated. The solid lines are 2nd order polynomial least squares fits to the data points. The location of the maximum of the fit provides the distance of the roof edge from the best focal position. If we assume the roof edges were placed correctly, this figure shows a small astigmatism in the telescope. This was consistent with the early measurement of the telescope with a Zygo interferometer before the IDA was assembled onto the telescope. The data also suggests that such small astigmatism will have little impact on the star tracking sensitivity.

Fig. 4a and 4b show the results of the field of view scan at room temperature for the x and y axis scan respectively. The result will be discussed later with the low temperature result. P0229 describes the procedures for performing the test as well as available data file names.

Fig. 5a and 5b show the results of the room temperature saturation range measurement for the x and y axis scan respectively. Data were collected in the range of 10 arc sec with steps of 0.1 arc sec. The differential of data for chan 1 and 2 for x axis and chan 3 and 4 for y axis plotted. The room temperature data is only used as a reference and the ultimate number used for meeting the specs is obtained at low temperatures. P0230 and P0231 are used for the procedures.

### **Low Temperature Test**

The cooling of the telescope started on March 9, 1998 with about 80 milli torr of helium exchange gas in the vacuum chamber. Liquid nitrogen was initially used for cooling the probe down to about 100 K over a period of 30 hours. Cooling from 100 K to about 4 K was performed in about 3 hours. A turbo pump is used to pump on the probe vacuum at all times to get rid of helium gas caused by a small low temperature leak in the probe.

After a helium transfer, some of the channels would not work properly. This was later found to be due to insufficient heating on the sapphire platform from the self heating of the FET's. When the platform heater was activated, we were able to make the circuits work reproducibly at all times. The missing data in certain channels in the results presented below are due to lack of heating on the thermal platforms.

The first sets of tests at low temperature are again for sanity check of the telescope. They consist of a wide field scan with the results shown in fig. 6a and 6b and a narrow field scan with the results shown in fig. 7a and 7b. The procedures and full data set are described in P0235 and P0236, respectively. The wide field scan shows that in addition to the sloped top in the Y axis channels, there is also a small, but acceptable, sloped top in X axis channels along the Y scan direction. This might have been due to a misalignment of the DPA detector platform due to cryo distortion.

The focal scan, with the procedures described and data recorded in P0249 and its attachments, shows a similar result as that at room temperature. The summary scan result is shown in fig. 8.

### **Telescope Field of View**

*Specifications:*

*T003, 7.2.1:*

*The fused quartz telescope shall have a field of view, including the effects of telescope misalignment, so that at least 10% of the light from any star lying at an angular separation of less than 60 arc sec from the telescope null point on either of the axes reaches one of the photodetectors on that axis.*

*SIA spec:, 3.7.1.6.2.1.2.4*

*The aperture stop shall have a radius so as to include at least 10% of the light from any star at an angle less than 70 arc sec from the direction which centers the image of a distant star on the center of the aperture stop.*

The SIA is a fabrication spec which ensures that the T003 spec can be met optically.

The field of view scan is described and results recorded in P0237. The typical result is shown in fig. 9

The results in the P0237 shows that the all channels meet the spec by providing a field of view of ~ 75 arc sec except for negative direction of Y axis which gives about 55 arc sec. The fact that - Y axis has a much smaller field of view is believed to be a problem of DPA misalignment instead of a problem with the flight portion of the telescope. This is apparent by looking at fig. 1a where a symmetric field stop is observed on channel B detectors. No change of field of view is observed between room temperature and low temperature. This will be discussed later in the Discrepancies Observed section. The list below provides the measured field of view data averaged between the primary and redundant channels:

- + X axis: 75  $\pm$  0.5 arc sec
- X axis: 74  $\pm$  0.5 arc sec
- + Y axis: 76  $\pm$  0.5 arc sec
- Y axis: 55  $\pm$  0.5 arc sec

### **Telescope Saturation Range**

*Specifications:*

*T003, 7.2.2:*

*The fused quartz ST shall have a range of monotonic response (i.e., range over which the output signal monotonically increases with increasing angular deflection) of at least  $\pm 1$  arc sec.*

*SIA, 3.7.1.6.2.1.3:*

*The unsaturated range shall meet the requirements of Section 7.2.2 (of T003).*

The procedures and complete set of results are recorded in P0238. The slope of normalized signal is shown in fig. 10a and 10b for an x-axis and y-axis scans respectively. Also shown in the figures are vertical lines 1 arc sec away from the optical axis and zero slope line. The specs require data not to cross the zero slope line within 1 arc sec range. It is obvious from the graph that the specs are met.



## Telescope Perpendicularity of Readout Axes

### Specifications:

T003, 7.3:

*The two readout axes of the ST shall be orthogonal to each other to within 1 degree*  
SIA, 3.7.1.6.2.1.1

*The perpendicularity between the two readout axes shall meet the requirement of Section 7.3 of T003.*

The procedures and data sets used for analyzing the perpendicularity results are recorded in S0655 Rev.-. Due to the fact that the signal from orthogonal channels of the scan axis is not quite monotonic, as shown in fig. 14 a and 14b, the error bar in the result is relatively large (but adequate) compared with that in the test of Telescope #2. The reason for the non-monotonic signal is not clear. The result of 0.38 degrees +/- 0.20 degrees meets the spec.

## Telescope Linearity

### Specifications:

T003, 7.2.3

*The fused quartz ST shall have a linear range no less than  $\pm 60$  marcsec. The linearity error over the linear range shall not exceed 3.0 marcsec.*  
SIA, 3.7.1.6.2.1.4

*The linear range and linearity shall meet the requirements of Section 7.2.3 assuming a model function to map signal into angle.*

The linearity requirement shall be met by analysis. The test performed here is only for checking potential anomalies in the telescope signal. To the extend the measurement can be made, no anomaly was observed.

P0240 provides the data for the linearity measurement and analysis. Due to lack of signal average, the linearity error from the measurement is  $\pm 10$  marcsec on X axis and  $\pm 40$  marcsec on Y axis in the  $\pm 60$  marcsec range. The error is larger in Y axis because the air conditioner was turned off in the lab to see the effect of temperature on the measurement noise. To reduce the noise to the required spec, about 10 days of data collection is required on each axis. For the current test, the schedule made it impossible.

## Telescope Strehl Ratio

### Specifications:

SIA, 3.7.1.6.2.1.5

*The Strehl Ratio shall be  $\geq 72\%$ .*

The total Strehl ratio including the telescope, the star and the windows is measured by comparing the slope data with the calculated data. The total Strehl is  $93\% \pm 1\%$  while the Strehl of the star was measured to be  $97\% \pm 1\%$  and that of cryogenic windows was  $92\% \pm 1\%$  by using the formula  $S.R. = \exp[-(2\pi\varnothing)^2]$ , where  $\varnothing$  is the r.m.s. wavefront error of the corresponding system. From these numbers, we see that the deduced the Strehl ratio would be  $104\% \pm 1\%$  which is not reasonable. This is probably because certain systematic wave front error compensated each other. However, the data collected at room temperature and 4 K showed no difference in total Strehl ratio within the measurement uncertainty. Therefore, we can use the Strehl ratio measured with an Zygo interferometer

at room temperature as the low temperature number for the telescope. That number is  $93\% \pm 1\%$  which is well above the requirement. P0241 is used for the data analysis.

### Telescope Scale Factor

#### Specifications:

##### T003, 7.4.1

*After initial ground calibration, the scale factor shall be known to within 20%.*

The scale factor SF is defined as:

$$\theta = SF [(I_+ - I_-)/(I_+ + I_-)]$$

Fig. 11a & b shows the scale factor as a function of  $(I_+ - I_-)/(I_+ + I_-)$  for both X and Y axis. The solid lines show the theoretical calculations. Keep in mind that all these results are for a single wavelength of 685 nm.

In fig. 11c, the dashed line shows the simulation result with the star spectrum of HR8703 as well as the spectra response of the photodiode taken into account. The dash dotted lines indicate 20% deviations from the HR8703 scale factor curve. This indicates that the 685 nm scale factor curve is well within 20% of the scale factor if the real star is used. No change in scale factor is observed between room temperature and low temperature.

P0245 provides the detailed procedure on how the analysis is performed.

The scale factor which provides the actual current per unit angle movement can only be provided by analysis after the information of the flight detectors and windows become available.

### Telescope Optical Transmission

#### Specifications:

##### SIA 3.7.1.6.2.1.6

*The power transmissibility collectively to all of the photodetectors shall be greater than or equal to 20% of the total light incident on the clear aperture of the telescope over an optical bandwidth from 400 nm to 1000 nm.*

The procedures for measurement and data analysis are given by P0247.

The total input power is obtained by doing a raster scan of a power meter sensor head over a 6" x 6" area. The scan result is shown in fig. 12. The result is integrated in the telescope clear aperture area to give the total input power to the telescope which is 16.87 nW. The windows transmission is measured to be  $44\% \pm 5\%$ . Since the total change of the end-to-end transmission from room temperature to 4 K is 2%, we'll use the value at room temperature for 4 K without much loss of precision. Assuming a quantum efficiency of 0.47 A/W at 685 nm for the photodetectors, the total transmission including the windows is 12% and excluding windows is  $27\% \pm 2\%$ .

Notice that due to the fact that the window transmission changed very little between room temperature and 4 K, we were able to make an absolute measurement of the total transmission.

## Telescope Orientation of Reticle Reflecting Surface

### Specifications:

#### SIA 3.7.1.4.3.4

*The perpendicular to the reflecting surface of the reticle plate shall be parallel to the telescope optical axis within 10 arcsec and be known to within 5 arc sec.*

Since the release of the procedure, a method has been found to measure the angle in an absolute manner. Therefore, there was considerable redlining in P0246 which governs the measurement and analysis of the angle.

The basic idea is to set up the star for a normal incident angle to the reference mirror inside the star. This is done by adjusting the PZT which controls the diagonal mirror so that the return image of the light source falls back onto itself. This can be done easily within 1 arc sec and is the major source of the error. The PZT position is recorded as position 1. The servo is then turned on and providing PZT position 2. The telescope reticle plate is then aligned parallel to the reference mirror of the star by adjusting the telescope so that the servo system would lock on to PZT position 2. With the servo off and PZT set to position 1, the star beam is then steered so that the incident beam is along the optical axis of the telescope. The amount we have to steer between the last two positions is the angle we intend to measure.

The angle of the perpendicular of the reticle plate and telescope optical axis was measured to be 8.7 arc +/- 1.4 arc sec at 4.2 K and 4.6 arc sec +/- 1.4 arc sec at room temperature.

If we take the optical axis to be along the z axis of ACS (see Appendix A for the definition of ACS), the normal vector of the coated side of the reticle plate lies in the 1st quadrant of the ACS. The x and y components in the ACS of the angle between the normal vector and z axis is:

x-component projection:  $7.4 \pm 1.0$  arc sec (rotation about y axis:  $7.4 \pm 1.0$  arc sec)

y-component projection:  $4.6 \pm 1.0$  arc sec (rotation about x axis:  $-4.6 \pm 1.0$  arc sec).

## Misalignment of Optical Center from Center of Aperture Stop

### Specifications:

#### SIA 3.7.1.6.2.1.2.1

*The misalignment of the optical center of the telescope is defined to be the angle between the direction to a distant star which centers the image of the star on both of the image splitting roof prisms and the direction to a distant star which centers the image of the star on the center of the aperture stop. This misalignment shall be less than 10 arc sec.*

The data for the misalignment is obtained by analyzing the data for the field of view as in fig. 9. The number obtained was 10.9 arc sec. This number is not meeting the specification. However, we believe this is due to a misalignment problem in the DPA. This will be discussed further in Discrepancies Observed section.

### **Telescope Readout Noise Performance and Related Telescope Data**

The DPA's used in this test are engineering models whose beam splitters are different from the flight models in that they have silver instead of aluminum coatings and the splitting ratios are not 1:1. Therefore the measurement performed here is only for future reference rather than for demonstrating the performance.

All the data collected are on channel B transmitted + detector. Observations on the noise performance were made on other channels and some of the channels are worse by a factor of 2 or 3. Since very little time was spent on such noise measurement, I cannot be quantitative about the performance of other channels. It was apparent that the channel on which the noise measurement was made has the lowest noise.

For all the noise measurement, no light was used. The sampling rate for the data collection was at 5 ksps and 300 points in the middle of the 0.1 sec reset interval were used for a least squares fit to obtain the voltage ramping rate. This along with the gain factor and feedback capacitance values will give the current. 1000 such current values were used for a histogram. A Gaussian fit to the histogram provides the noise value. 10 such noise values were used for an average. The noise value is then converted to  $\text{aA}/\sqrt{\text{rtHz}}$  by dividing the number by  $(10)^{1/2}$ . This measurement is made for a temperature range from 40 K to 120 K with a temperature increment of  $\sim 10$  K. The result is shown in fig. 13. If 10 fA of peak photocurrent is expected on each photodiode for the guide star, divide the noise by 52 fA/arc sec would give the pointing noise in  $\text{arc sec}/\sqrt{\text{rtHz}}$  for a Strehl ratio of 93%.

A measurement is also made with very low light intensity for the telescope. This was only to see if there is any unexpected behavior from the telescope when the light level drops to very close to that of the guide star. Fig. 14 shows the scan result. No unexpected behavior is observed.

With all the detectors operating, the temperature of the forward plate of the telescope is measured to be 7 K while the base plate is held at 4 K.

### **Discrepancies Observed**

As mentioned in the previous sections, two of the specifications were not met by the test of the telescope. These along with other unexpected behaviors will be discussed here.

First, all the channels do not have the same peak intensity as demonstrated in fig. 4 and fig. 9. This problem, if not corrected, could potentially affect the pointing signal to noise ratio in lower intensity channels. Therefore, some tests should be repeated with the flight detectors. Table 1 lists all the peak intensity readings for each channel as well as the intensity relative to channel 1 peak at the given temperature. It is apparent that the ratios do not change much between room temperature and 4 K. There appears to be an intensity splitting ratio of 1:3 for the beam splitters inside the DPA with a lower reflected side intensity. A similar beam splitter has been measured to have a splitting ratio of about 1:2 with less light going reflected side which qualitatively agrees with the telescope result. The difference between channel A and channel B cannot be completely understood at the moment. Some of it may be due to a polarization effect.

Table 1. Peak Intensity Distribution of All Detectors

Channel #	I (RT) (pA)	I(RT)/I1(RT)	I(4K) (pA)	I(4K)/I1(4K)
1	292.4	1	291.4	1
2	259.5	0.89	255.9	0.88
3	83.8	0.29	81.1	0.28
4	143.1	0.49	139.5	0.48
5	34.8	0.12	32.8	0.11
6	55.6	0.19	-	-
7	110.2	0.38	107.5	0.37
8	102.4	0.35	98.7	0.34

The second problem observed is that the telescope response is not flat in the region where all the light is supposed to be centered on one of the photo detectors in channel A. The signal level changes by about 15% across the field on each detector. This is shown in fig. 4b as well as fig. 1b. Upon cooling down to 4 K, a similar, but smaller, effect is observed also on channel B, as shown in fig. 6a. The effect on channel B disappears upon warming up to room temperature, indicating that there might be a problem with cryogenic straining of the detector package. The effect on channel A can be qualitatively reproduced in a setup in the telescope assembly clean room. It is still not well understood what is the nature of the problem. This problem, if not corrected, might not have any impact on the performance of the telescope as long as the effect is not time dependent.

The above two problems were reported in DR 125.

The third problem is that the field of view does not meet the specification on channel A + detectors. This is most likely caused by misalignment of the photodiodes on the DPA with respect to the light beam. The falling edge of the telescope signal on channel 3 or channel 5 in fig. 4b is very sharp compared to other channels. This indicates the signal is not clipped by the field stop of the telescope which gives a very slow falling edge. This problem can be corrected by a better alignment method for the DPA on the telescope when the flight detectors are to be mounted. Even if this problem is not corrected, it should not have an impact on the telescope performance during normal operation. It might increase the initial star searching process slightly. This problem is reported in DR 129.

The last problem observed is the existence of dust particles on the telescope forward plate as well as inside the metering tube. The telescope has since been cleaned. The cause of the contamination is under investigation. With the telescope cleaned, this problem will not have any impact on the performance of the telescope. This problem is reported in DR 134.

**Summary**

The telescope #3 have been tested both at room temperature and at low temperature. All but one specification intended to be tested in the test plan described in P0254 have been met. The specification which is not met is the field of view. This problem will most likely be corrected with the flight detectors, but will have little impact even if not corrected. Other discrepancies can either be corrected easily or will have little impact on the performance of the telescope.

## Appendix A.

### Telescope Detector Assignment and Scan Coordinate Cross Reference

In this appendix, the test configurations in artificial star are referenced to the absolute coordinate system (ACS) provided in GP-B Dwg 23521 Rev. A released on May 28, 1998.

The notations used in the table below are interpreted as follows:

- SX: Image movement along ACS X direction.
- SY: Image movement along ACS Y direction.
- RX: Rotate telescope about ACS X axis. The direction is defined by the right hand rule.
- RY: Rotate telescope about ACS Y axis.
- WX: Wide field scan X direction.
- WY: Wide field scan Y direction.
- NX: Narrow field scan X direction.
- NY: Narrow field scan Y direction.
- CH#: A/D card channel number.
- IDA\_TR: Transmitted light in the IDA (Image Divider Assembly).
- IDA\_RF: Reflected light in the IDA.
- DPA\_TR: Transmitted light in the DPA (Detector Package Assembly) with the signs provided by TRE.
- DPA\_RF: Reflected light in the DPA with the signs provided by TRE.
- CH@: Channel A or B as designated by GP-B DWG 25445 Rev. A and GP-B DWG 25444 Rev. A released on Jan. 27, 1998.

Table A1. Cross Reference

CH#	IDA	CH@	DPA	W	N	R	S
1	IDA_TR	B	DPA_TR+	WX-	NX-	RXccw	SY-
2	IDA_TR	B	DPA_TR-	WX+	NX+	RXcw	SY+
3	IDA_RF	A	DPA_TR+	WY-	NY+	RYcw	SX-
4	IDA_RF	A	DPA_TR-	WY+	NY-	RYccw	SX+
5	IDA_RF	A	DPA_RF+	WY-	NY+	RYcw	SX-
6	IDA_RF	A	DPA_RF-	WY+	NY-	RYccw	SX+
7	IDA_TR	B	DPA_RF+	WX-	WX-	RXccw	SY-
8	IDA_TR	B	DPA_RF-	WX+	WX+	RXcw	SY+

***FIGURES TO S0300 REV. A***

(Same as from S0300 Rev. -)  
June 15, 1998



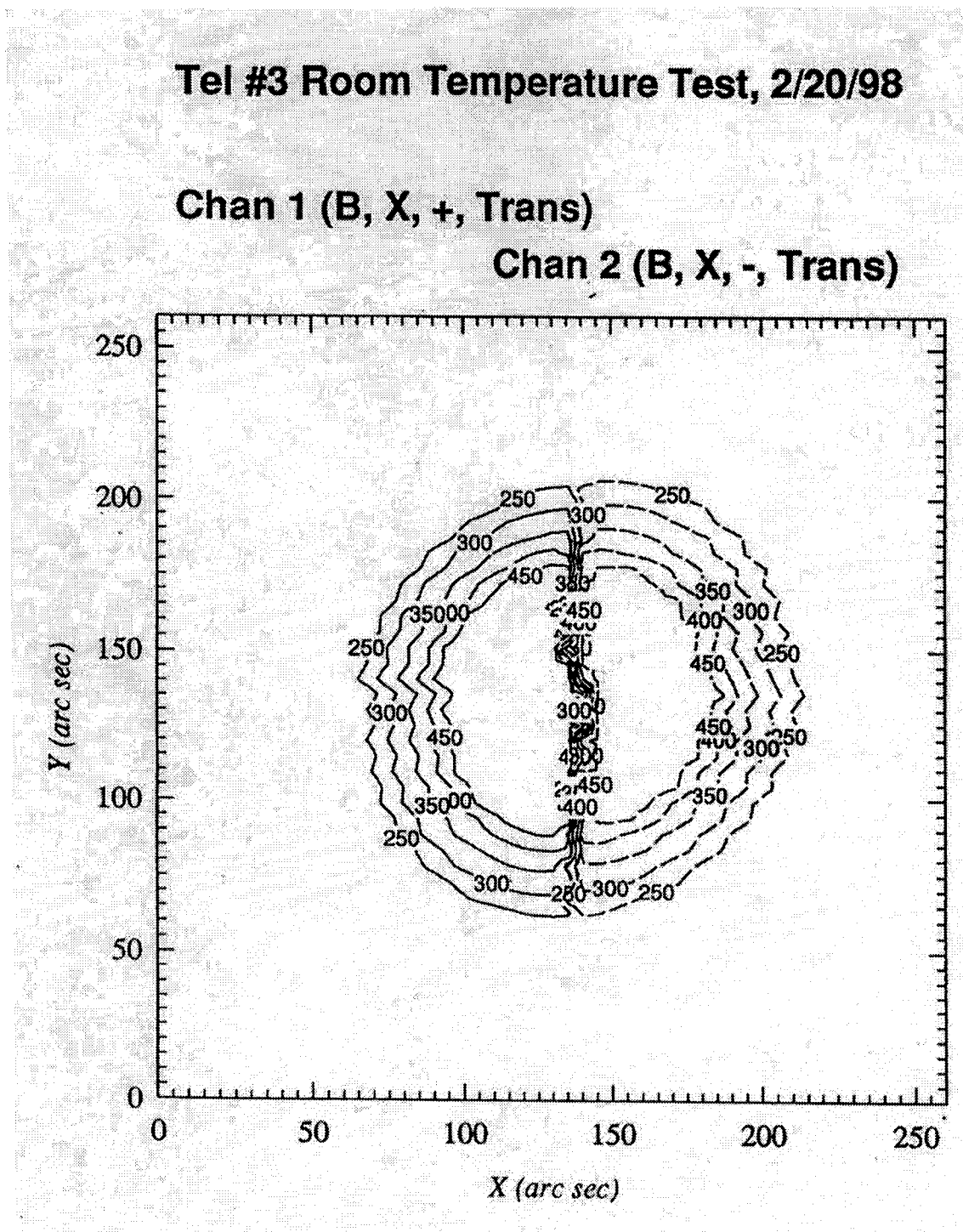


FIGURE 1A

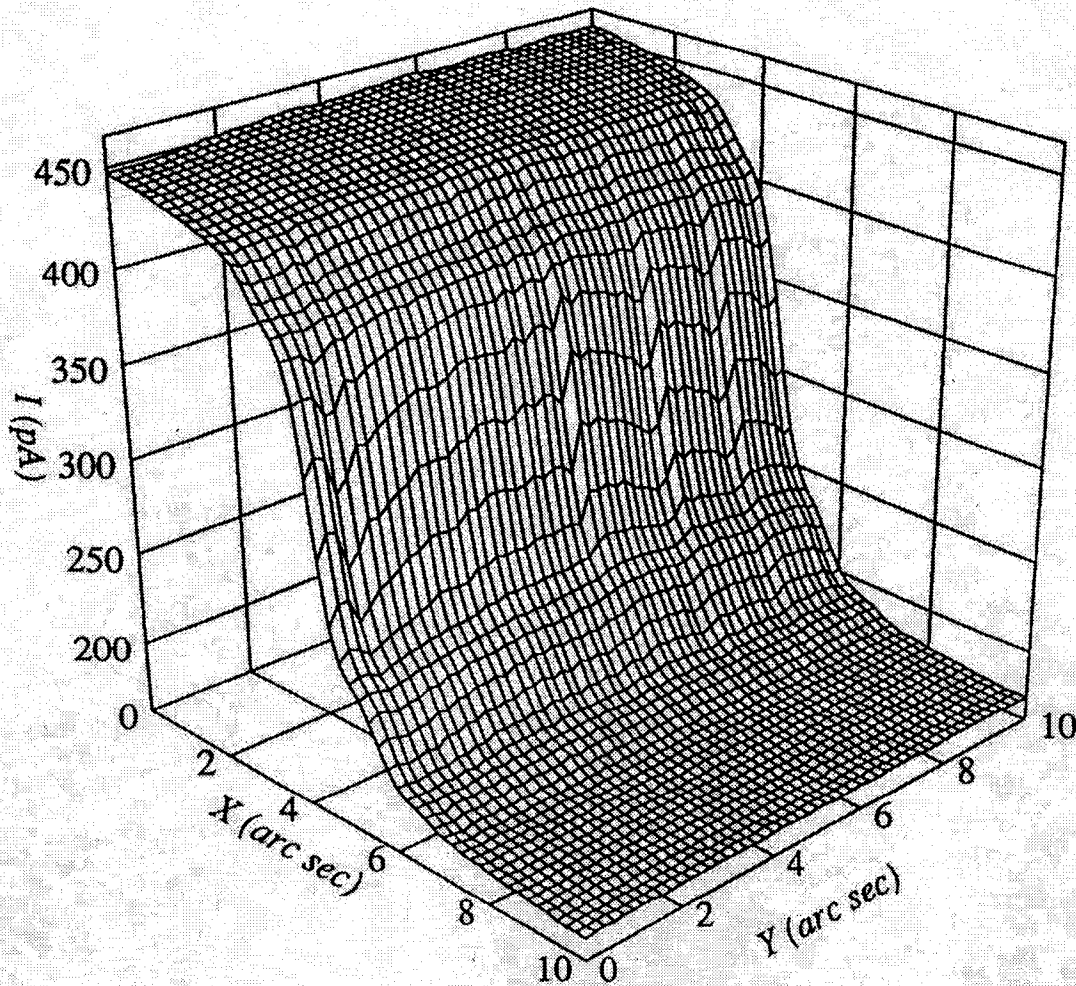
**Tel #3 Room Temperature Test, 2/24/98****Chan 1 (B, X + Trans)**

FIGURE 2A

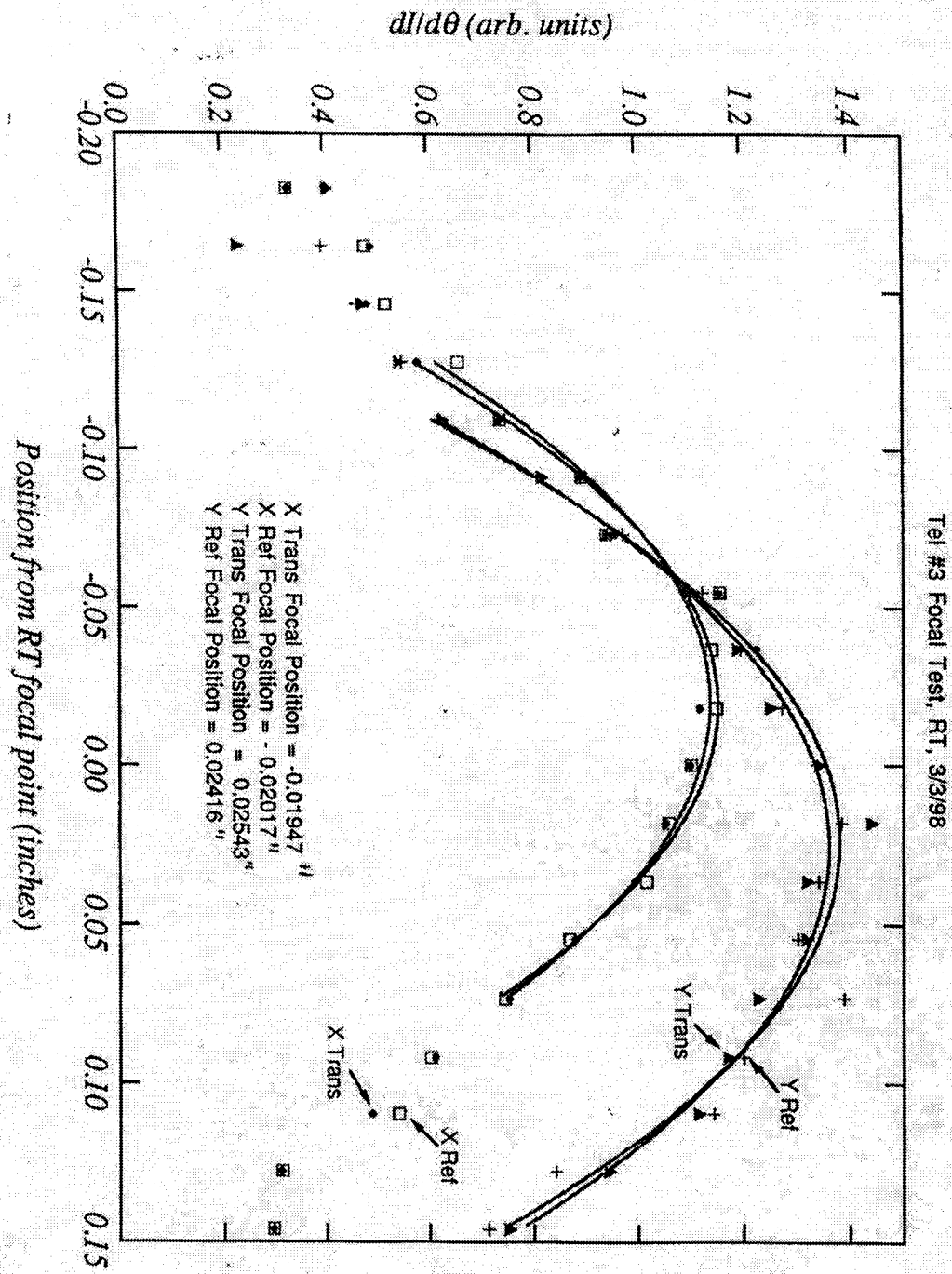


FIGURE 3

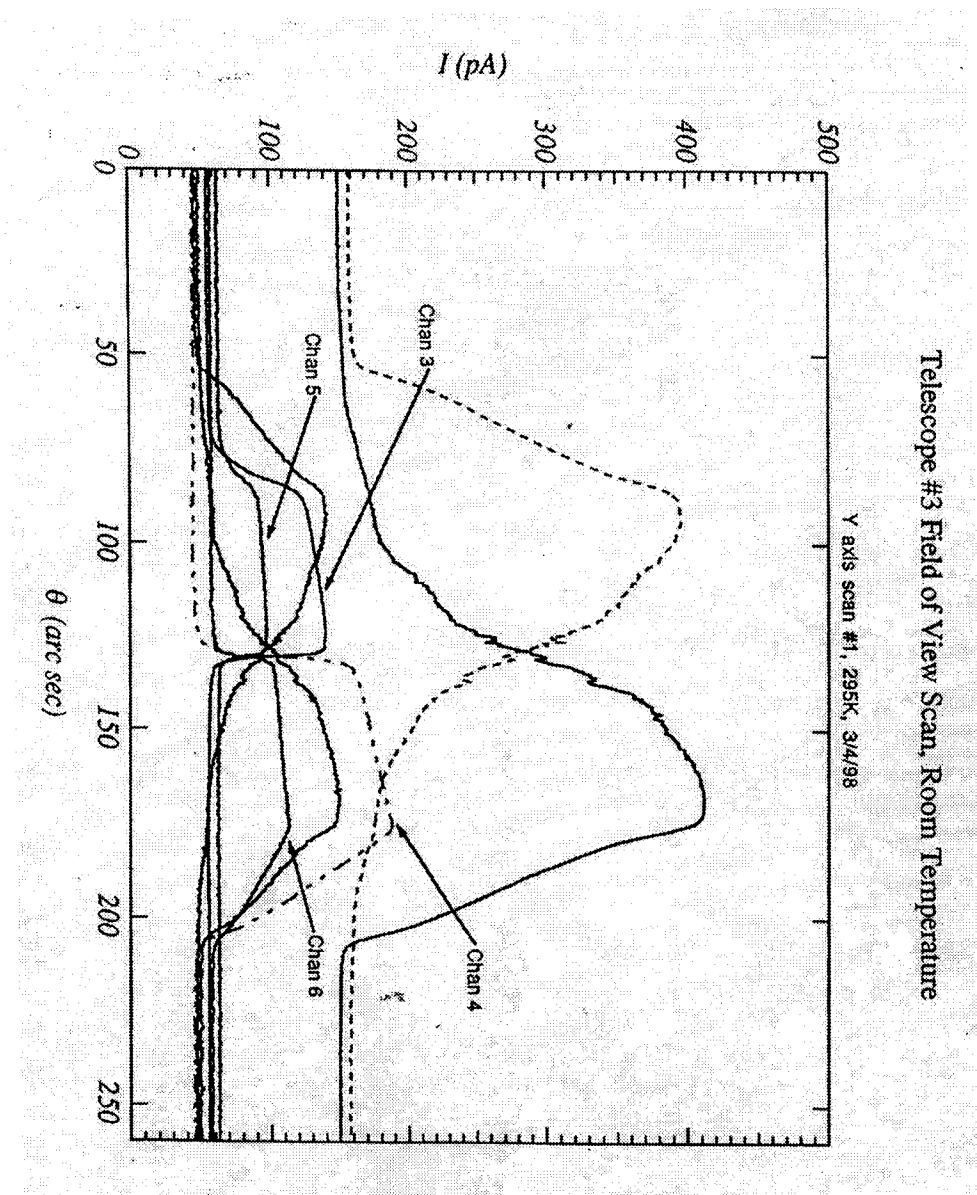


FIGURE 4B

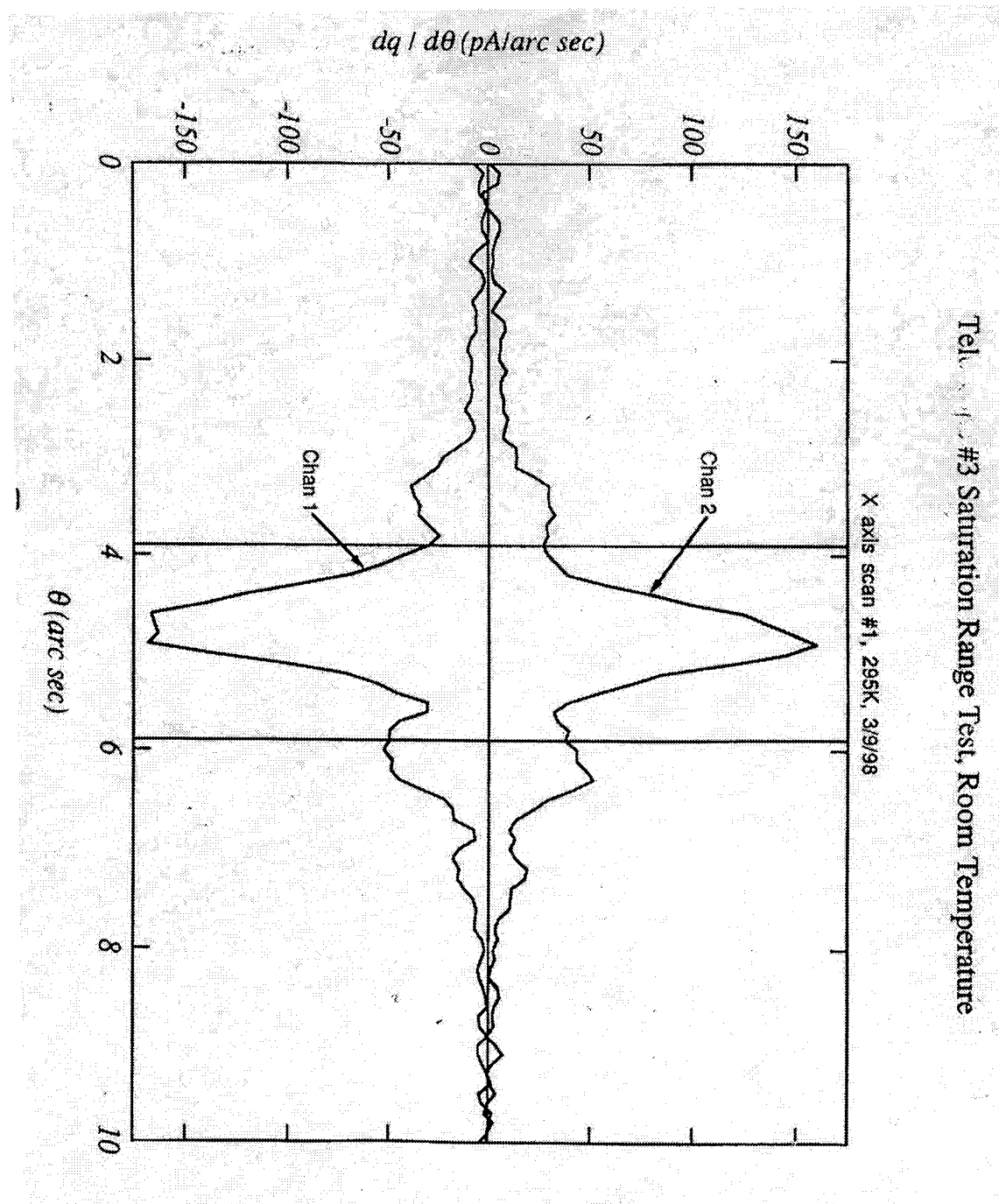
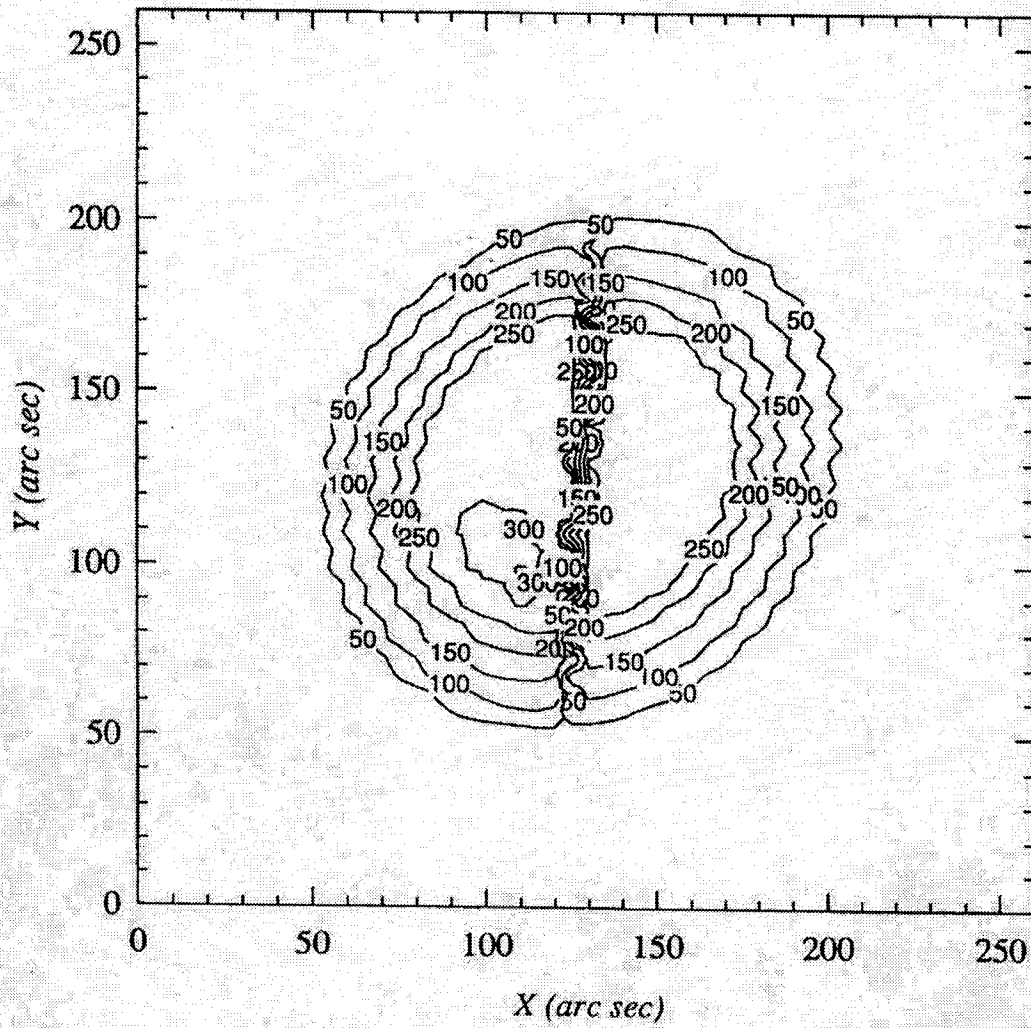


FIGURE 5A

**Tel #3 Wide Field Scan, 4K, 3/12/98****Chan 1 (B, X, +, Trans)****Chan 2 (B, X, -, Trans)****FIGURE 6A**

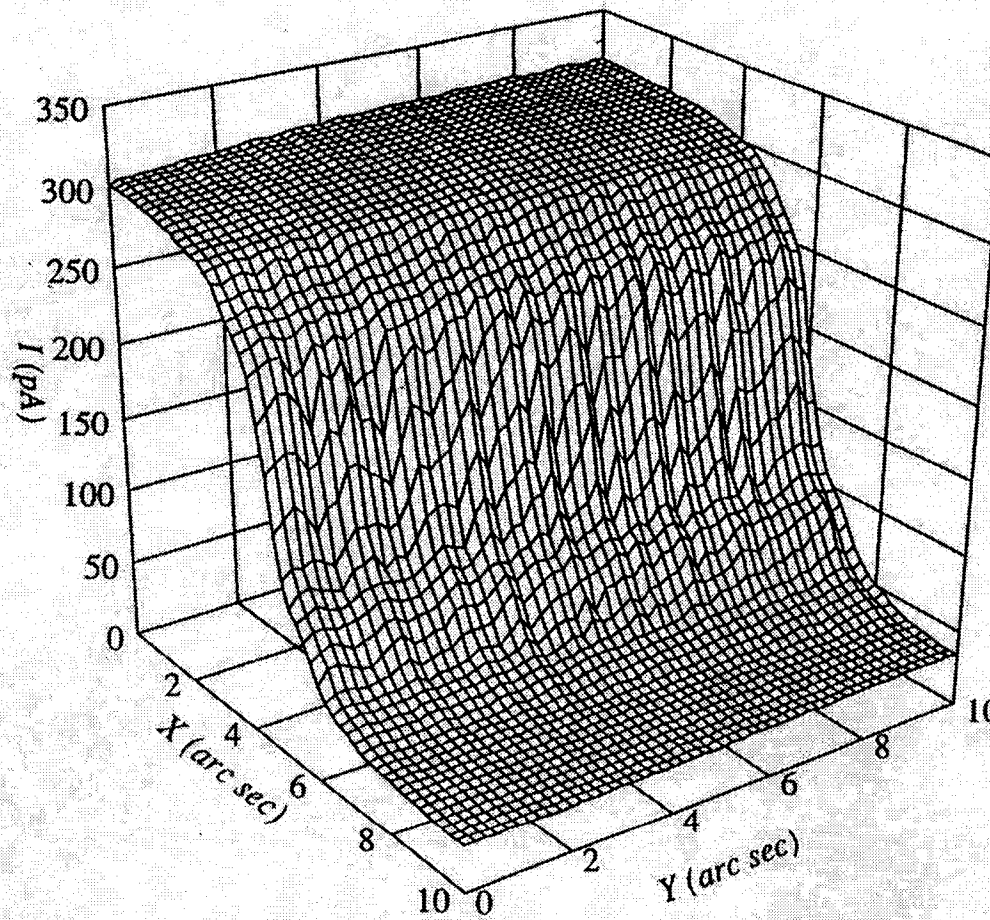
**Tel #3 Narrow Field Scan, 4K, 3/25/98****Chan 1 (B, X + Trans)**

FIGURE 7A

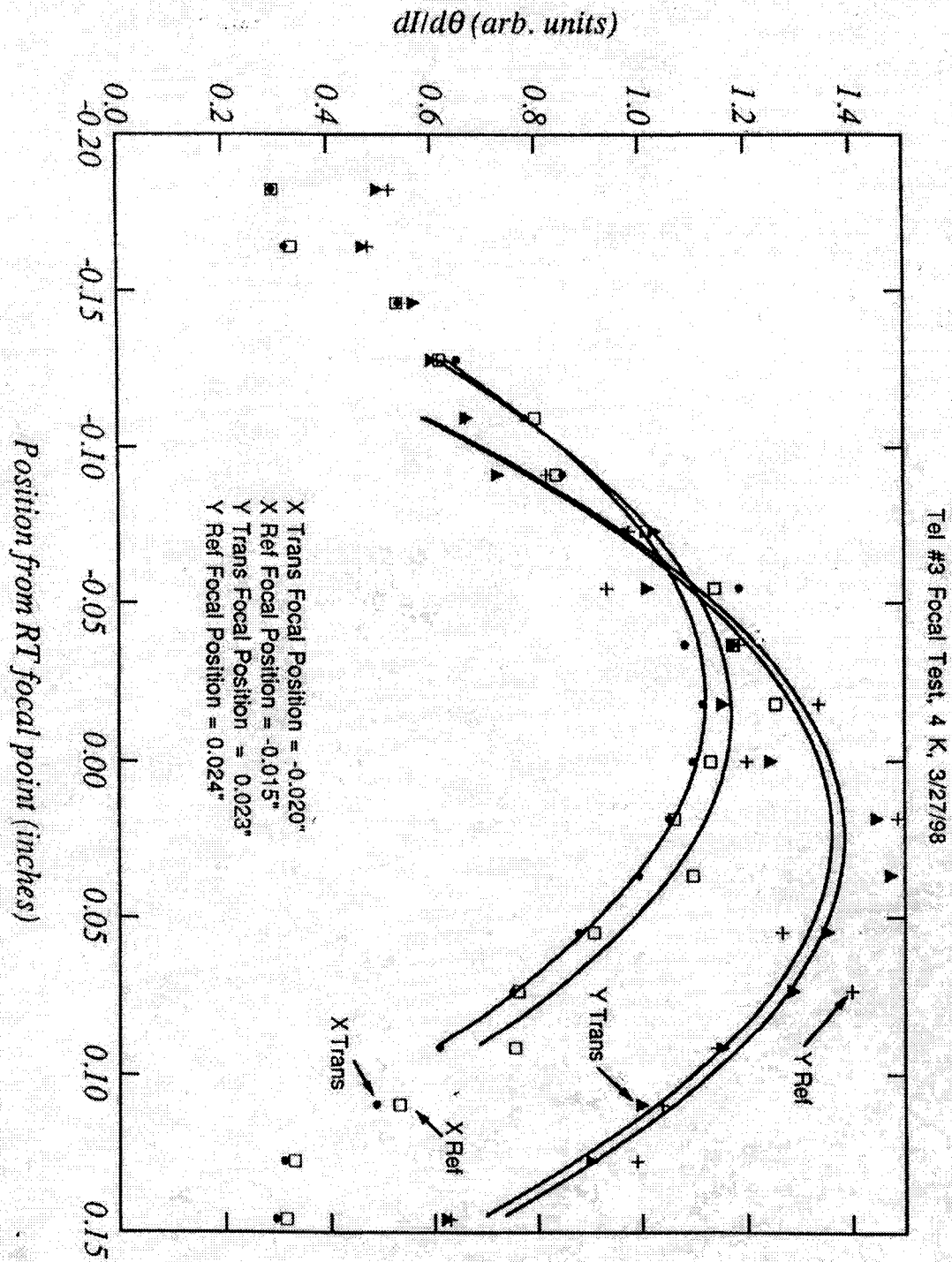


FIGURE 8



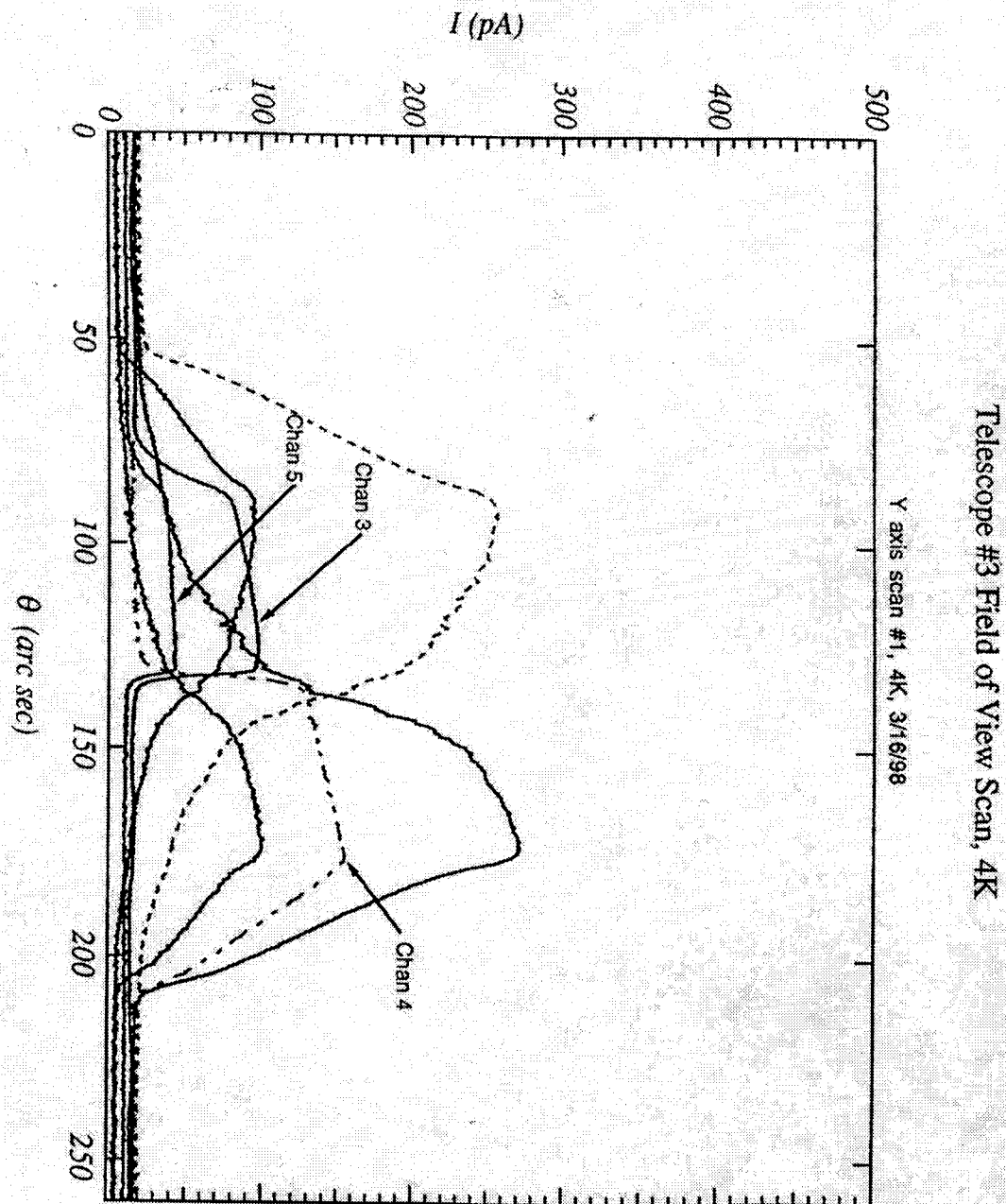


FIGURE 9B

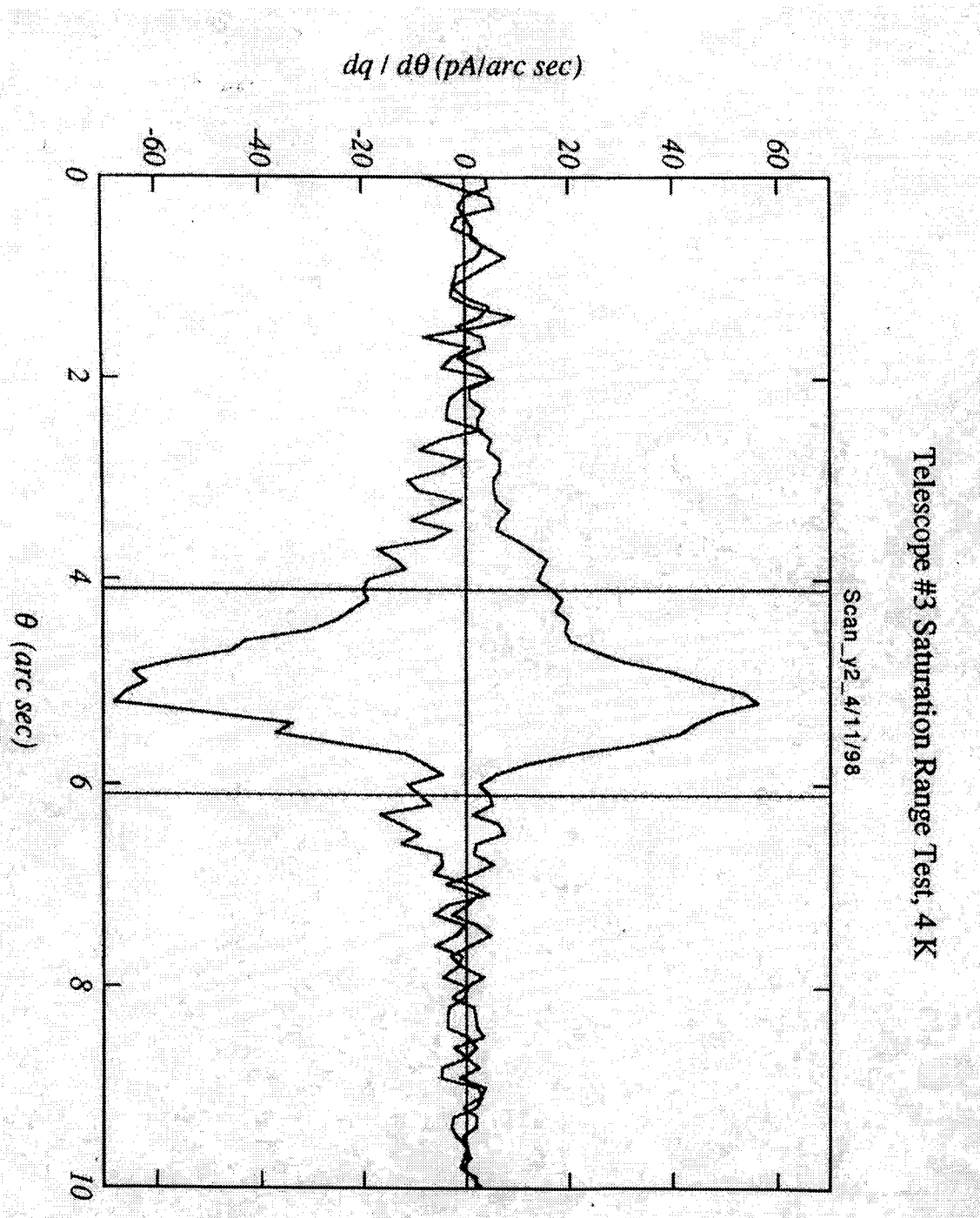


FIGURE 10B

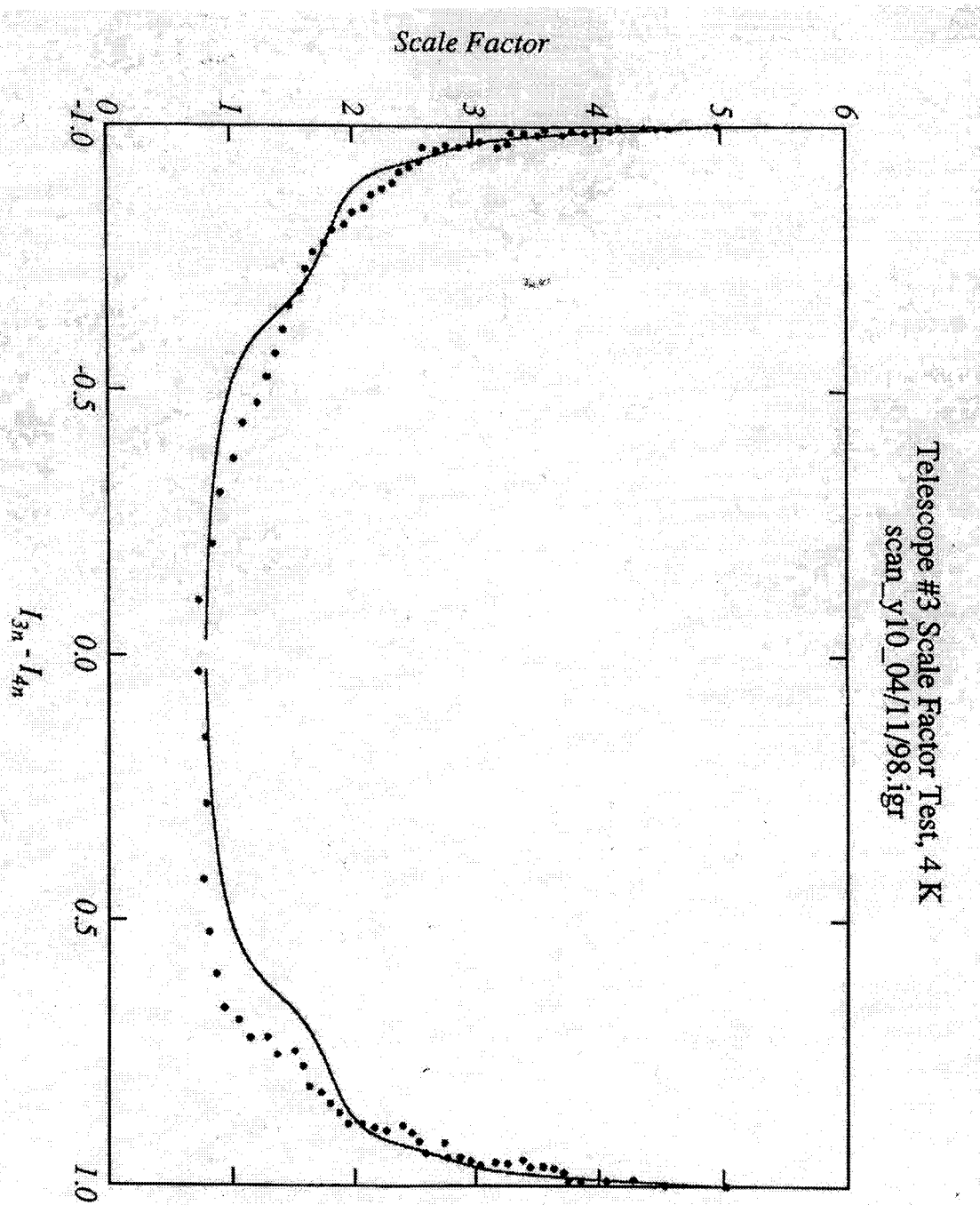


FIGURE 11B

**Telescope #3 Test**  
**Artificial Star #2 Intensity Measurement**  
**4/30/98**

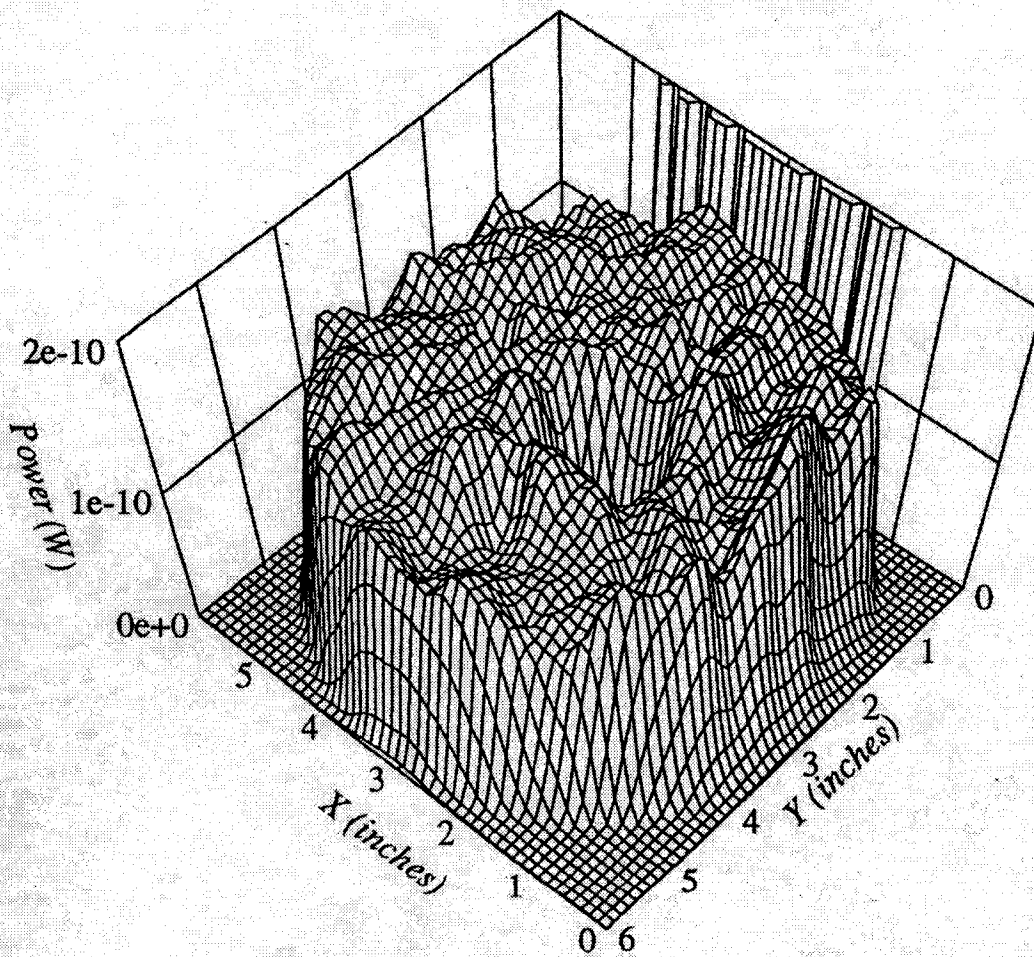


FIGURE 12A

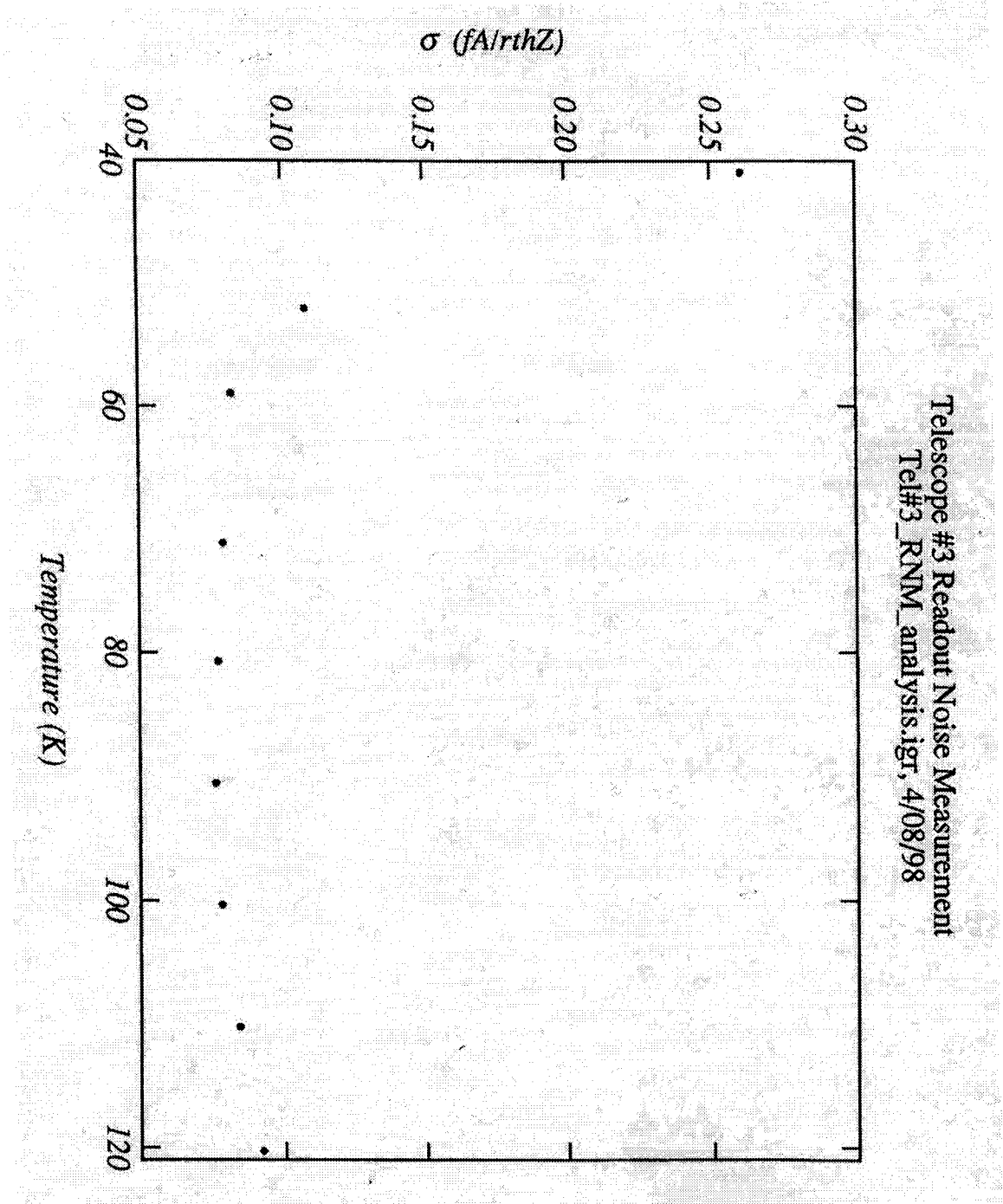


FIGURE 13

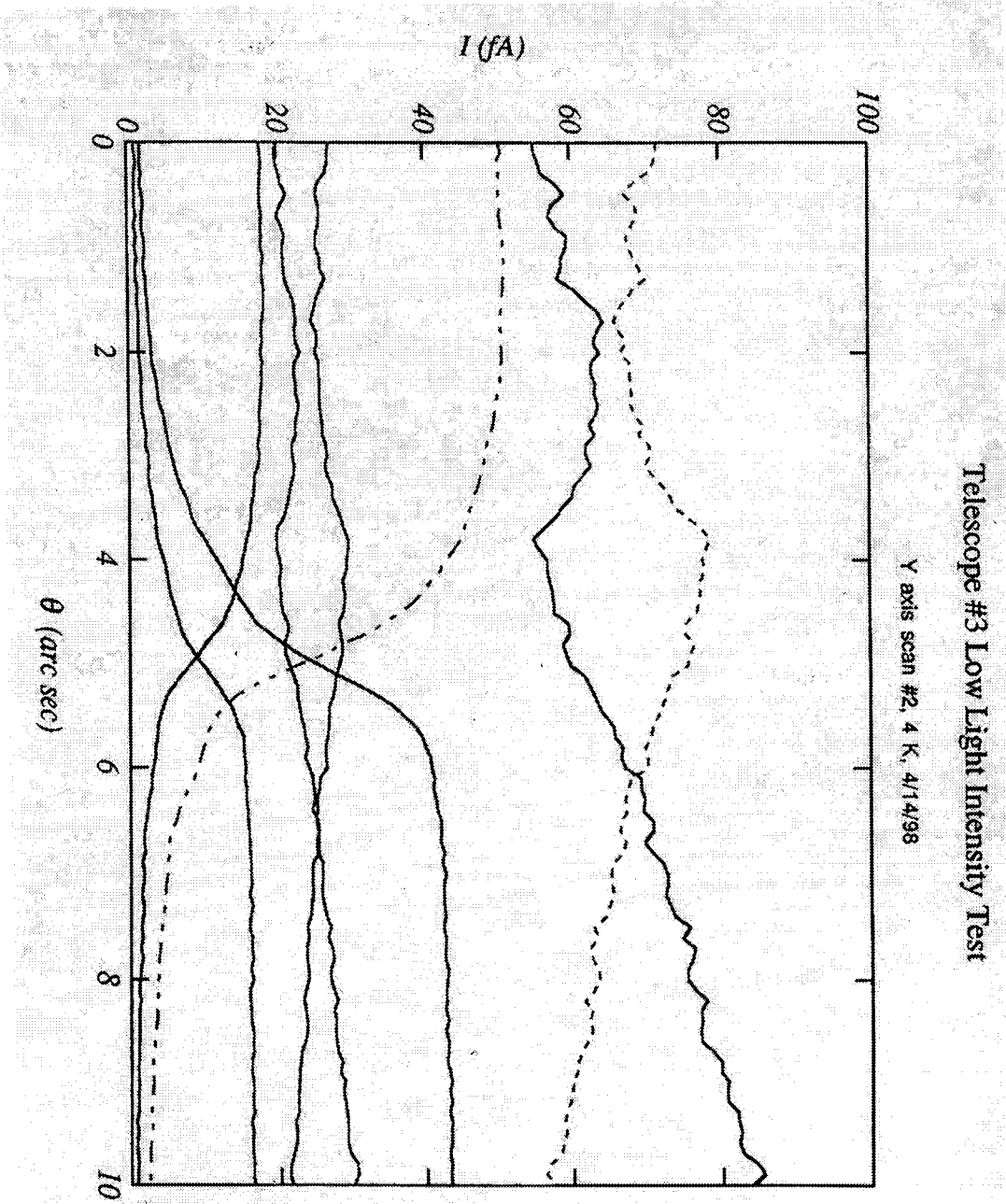


FIGURE 14B